Parasympathetic-Sympathetic Causal Interactions Assessed by Time-Varying Multivariate Autoregressive Modeling of Electrodermal Activity and Heart-Rate-Variability

Alejandro Luis Callara, Laura Sebastiani, Nicola Vanello, Enzo Pasquale Scilingo, and Alberto Greco

***Abstract*—*Objective:* Most of the bodily functions are regulated by multiple interactions between the parasympathetic (PNS) and sympathetic (SNS) nervous system. In this study, we propose a novel framework to quantify the causal flow of information between PNS and SNS through the analysis of heart rate variability (HRV) and electrodermal activity (EDA) signals. *Methods:* Our method is based on a time-varying (TV) multivariate autoregressive model of EDA and HRV time-series and incorporates physiologically inspired assumptions by estimating the Directed Coherence in a specific frequency range. The statistical significance of the observed interactions is assessed by a bootstrap procedure purposely developed to infer causalities in the presence of both TV model coefficients and TV model residuals (i.e., heteroskedasticity). We tested our method on two different experiments designed to trigger a sympathetic response, i.e., a hand-grip task (HG) and a mental-computation task (MC). *Results:* Our results show a parasympathetic driven interaction in the resting state, which is consistent across different studies. The onset of the stressful stimulation triggers a cascade of events characterized by the presence or absence of the PNS-SNS interaction and changes in the directionality. Despite similarities between the results related to the two tasks, we reveal differences in the dynamics of the PNS-SNS interaction, which might reflect different regulatory mechanisms associated with different stressors. *Conclusion:* We estimate causal coupling between PNS and SNS through MVAR modeling of EDA and HRV time-series. *Significance:* Our results suggest promising future applicability to investigate more complex contexts such as affective and pathological scenarios.**

***Index Terms*—EDA, HRV, TV-MVAR, heteroskedasticity, causal interactions, autonomic nervous system.**

I. Introduction

THE autonomic nervous system (ANS) is the primary mechanism to unconsciously regulate most of the bodily functions such as heart rate, respiratory rate, sudomotor activity, urination, and digestion [1]. The two branches of the ANS, i.e., the parasympathetic (PNS) and the sympathetic nervous systems (SNS), are generally recognized to exert antagonistic effects on the regulation of autonomic functions. However, this opposing interplay is not algebraically additive, but complicated interactions exist [2]. Indeed, plenty of experimental and clinical studies have demonstrated the presence of multiple interactions between PNS and SNS, which are regulated by different mechanisms at both central and peripheral levels [3], and are generally complex, nonlinear and frequently non reciprocal [4]. Studying the dynamics of such interactions could provide important information on the psychophysiological state of subjects as well on how their alterations may influence the development of various disorders, including cardiovascular, inflammatory, metabolic, neurological, and psychiatric diseases [3].

Peripheral physiological signals represent a window on PNS and SNS functions. In this context, the heart-rate variability (HRV, [5]) and the electrodermal activity (EDA [6], [7]) can be considered the two main tools for noninvasively assessing the ANS dynamics [8]. Particularly, the spectral features of HRV and EDA have been found to be reliable markers of sympathetic and/or parasympathetic activity [4], [9]. The high-frequency components (HF, 0.15-0.4 Hz) of HRV spectrum are known to be primarily influenced by the parasympathetic activity [4], [5]. On the other hand, at low frequency (LF, 0.05-0.15 Hz) the HRV dynamics are driven by both PNS and SNS, and, consequently, it cannot be identified an exclusive sympathetic contribution in the HRV spectrum. Conversely, the EDA signal is known to reflect only sympathetic activity, as the sudomotor activity generating it is controlled only by the SNS [10], [11]. EDA spectral power components related to the SNS activity have been recently derived: i.e., the EDASymp and the TVSymp, defining the frequency range of the main sympathetic contribution to the EDA signal [12], [13].

Starting from these two ANS correlates, indexes describing the balance between the PNS and the SNS and the related physiological interpretation have been proposed, e.g. the LF/HF and the EDASymp/HF [4], [14]. Yet, a full characterization of the dynamics involved in coupled systems requires not only accurately quantifying the presence or absence of interactions, but also identifying driver-response relationships, in order to estimate the directionality between the two signals [15]. In this context, multivariate autoregressive (MVAR) models are probably the most widely used methods for characteriz-

A. L. C., N. V., E. P. S. and A. G. are with the "Dipartimento di Ingegneria dell'Informazione", University of Pisa, Via G. Caruso 16, 56122 Pisa, Italy and with the Research Center "E. Piaggio", University of Pisa, Largo Lucio Lazzarino 1, 56122 Pisa, Italy.

L. S. is with the "Department of Physiology and Biochemistry" "G. Moruzzi", University of Pisa, Via S. Zeno 31, 56127 Pisa, Italy.

The research leading to these results has received partial funding from the Italian Ministry of Education and Research (MIUR) in the framework of the CrossLab project (Departments of Excellence).

This research has received partial funding from European Union Horizon 2020 Programme under grant agreement n 824153 of the project "POTION-Promoting Social Interaction through Emotional Body Odours".

Corresponding author: alejandro.callara@ing.unipi.it.

ing such causal interactions [16], [17]. MVAR models extend to the multivariate case the concept of Granger Causality (GC) [18], [19], whose principle of causality is expressed in terms of temporal predictability. Accordingly, if the prediction error of a time series is significantly reduced by including another time series in the regression model, then the second series is said to have a causal influence on the first time series.

The original formulation of GC was proposed for wide-sense stationary linear stochastic processes [19]. Nevertheless, physiological time-series do not generally satisfy such conditions. For instance, interactions can be linear and nonlinear, and may vary over time. In this scenario, while the linear approximation was found to be satisfactory enough to detect GC between linearly and nonlinearly coupled time-series [20], [21], nonstationarity is known to produce spurious regression results [22]. To tackle this issue, time-varying (TV) solutions for estimating MVAR parameters were proposed: e.g. moving window approaches [23], recursive-least-squares (RLS, [24]) and Kalman filter [25]. Moreover, as TV-MVAR may exhibit TV residual variances (i.e., heteroskedasticity), adaptive algorithmic approaches to track optimally both model coefficients and residuals changes have been recently developed [16].

An attractive property of MVAR models for physiological time-series analysis is that they can be represented in the frequency domain [26]. Since biological systems usually operate through specific frequency bands, a frequency-domain description of their interactions is essential [4], [12], [27]. Generally, the transition from time-domain to frequency-domain is performed via the Fourier transform of MVAR model coefficients, followed by a normalization of the transformed coefficients. Based on the normalization procedure, different measures with different physiological meaning can be obtained (exhaustive reviews of these methods can be found in [26], [28], [29]). Among these different measures, the Directed Coherence (DC, [30]) is one of the most informative measures based on GC [29]. This metric is a scale invariant representation of the GC in the frequency-domain [29] which formalizes causality in terms of transmitted power spectrum from one time-series to another. In particular, the scale invariance property improves the decision error rate of classified causal influence, and it is hence especially important in bootstrap-based approaches to test for significant causal interactions [31]–[33].

In the last decade, several applications of MVAR derived measures have been introduced in the cardiovascular domain for the characterization of the causal relationship among physiological mechanisms involved during cardiovascular regulation [34]. Particularly, most of these previous studies have modeled the relationship between heart period, systolic blood pressure and respiration [35]–[39]. In our preliminary study [40], we have proposed a first approach that used MVAR models applied to the spectral quantities of HRV and EDA to describe their interactions during a Handgrip task.

In this study, we apply a framework for the TV estimation of MVAR model coefficients and residuals [16], integrating physiological prior knowledge to assess the TV sympathovagal causalities from EDA and HRV. In particular, we exploit the frequency-domain representation of GC as implemented in the DC estimator to depict TV interactions between the sympathetic component of EDA and the parasympathetic component of HRV. Specifically, we integrate the causal profiles in their shared spectrum (i.e., 0.15-0.25 Hz). Furthermore, we control for heteroskedasticity of model residuals by introducing TV-variance stabilization in the DC estimates at each time-point. In addition, we extended the bootstrap approach of [32], [41] with the causal shuffling procedure presented in [33] to assess the statistical significance of observed causalities in the case of TV-MVAR model coefficients and TV model residuals. The methodology is applied and tested to two different tasks known to trigger a sympathetic response: a handgrip test and a mental computation task.

II. Materials and Methods

Parasympathetic-Sympathetic causal interactions were estimated for two different datasets obtained through two different experimental protocols: a handgrip task (HG) and a mental computation task (MC). Each protocol was applied to independent groups of healthy subjects. All participants provided written informed consent to take part in the research study. The experiments were approved by the "Bioethics Committee of the University of Pisa" (n. 3/2019).

A. Experimental protocols

1) Handgrip task: Twenty-six healthy subjects (aged 24 $\pm$ 2 years) were enrolled in this study. The protocol consisted of 5 minutes of resting state and 2 minutes of handgrip task. During the resting-state, subjects kept their eyes open for the first 3 minutes, and then they were advised to close them while maintaining relaxation. Finally, during the handgrip task, subjects were asked to tighten a small hard ball in his/her dominant hand at the maximum force of contraction. The ECG and EDA signals were recorded using the BIOPAC MP 150 system with a sampling frequency of 500 Hz.

2) Mental computation task: Twenty-four healthy subjects (aged 24 $\pm$ 2 years) were enrolled in this study. We purposely replicated the HG protocol timing. Thus, the experiment consisted of 3 minutes of eyes-open resting-state, followed by 2 minutes of eyes-closed resting-state and 2 minutes during which the subject was asked to perform a stressful mental computation task. Specifically, the instructions were to subtract, starting from 277, alternately 12 and 17 down to a 2-digit number, then multiply the obtained number by two and finally restart the series of subtractions. In case of error, the participant had to start the calculation again. The ECG and EDA signals were recorded using the BIOPAC MP 150 system with a sampling frequency of 500 Hz.

B. Physiological signal processing

R-peak consecutive intervals of each ECG signal were detected employing the well-known Pan-Tompkins algorithm [42] in order to generate RR time-series that were subsequently resampled at 4 Hz to derive the HRV signals.

Concerning the EDA signal, it can be split into two main components that are characterized by different time scale and

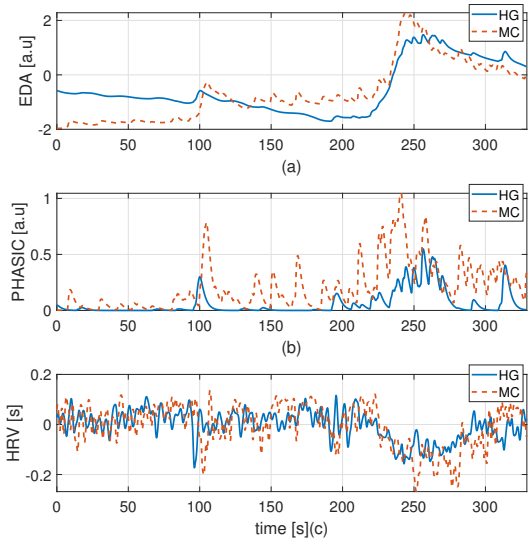

Fig. 1. Exemplary EDA, PHASIC and HRV signals for one subject. In blue, handgrip (HG) session signals. In red, mental computation (MC) session signals.

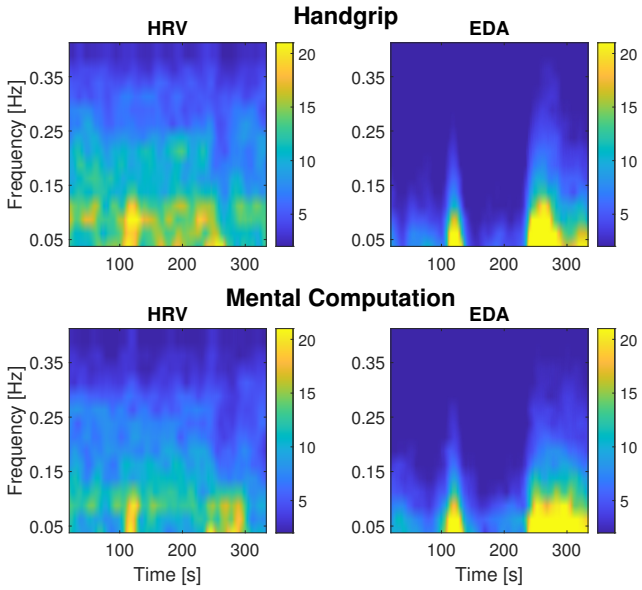

Fig. 2. HRV and EDA spectrograms. (top) Time-frequency PSD of HRV and EDA signals averaged over subjects during HG. (bottom) Time-frequency PSD of HRV and EDA signals averaged over subjects during the MC.

relationship to the triggering stimuli. The tonic component reflects baseline slow drifts, whereas the phasic component represents the short-term fast-varying response to external stimuli mediated by the SNS. In this study, we applied the cvxEDA model in order to extract the phasic response from the raw EDA signal [43]. The cvxEDA is a widely used approach that decompose the EDA signals through a rigorous methodology based on Bayesian statistics, mathematical convex optimization, and sparsity, without the need of pre- and post-processing steps. Indeed, the cvxEDA algorithm outputs include a white Gaussian noise term incorporating model prediction errors as well as measurement errors and artifacts. Finally, both HRV and EDA were normalized to have zero mean and unit variance for subsequent analyses. An exemplary EDA phasic decomposition, together with the associated HRV signal can be seen in Fig. 1. In Fig. 2, we also report the time-frequency representation of the power spectral density (PSD) of HRV and EDA time-series averaged over subjects in the two protocols. As expected, the frequency content of the two signals was modulated throughout the experiment. Particularly, both the HRV and EDA PSD were consistent during the resting sessions and change their frequency dynamics once the HG and MC tasks started. Moreover, the evident peak in the EDA PSD after around 110s corresponded with the closing of the subjects' eyes.

C. Parasympathetic-sympathetic causal interactions

We modeled the PNS-SNS linear causal interactions from EDA and HRV signals based on the following assumptions:

- The time delay between the SNS stimulation of the sweat glands and the EDA signal recording is not negligible and can be estimated as 1.62s based on physiological prior knowledge [44].
- The frequency range in which interactions between PNS and SNS given by the MVAR modeling of HRV and EDA time series are fully interpretable correspond to the spectral overlap between the EDASymp component (i.e., 0.045 - 0.25 Hz) of the EDA [12] and the HF component (i.e., 0.15-0.40 Hz) of the HRV [4], i.e., the (0.15-0.25) Hz frequency range. Indeed, at lower frequencies it is not possible to distinguish the type of interaction (i.e., $PNS_{HRV} - SNS_{EDA}$ vs. $SNS_{HRV} - SNS_{EDA}$), since the LF of HRV is influenced by both PNS and SNS.

Accordingly, prior to TV-MVAR model estimation, the EDA phasic signals were temporally shifted by -1.62s to consider the physiological delay between the SNS arousal activation and the EDA phasic response [44]. Taking into account this delay that is related to the sweat diffusion time, allows to correctly model the temporal predictability of the PNS and SNS, thus avoiding spurious and/or missing causal relationships between the two signals [45].

Afterwards, for each subject, HRV and phasic EDA time-series were used to construct bivariate autoregressive models from which the HRV-EDA bilateral interactions were explored. In particular, we estimated time-varying (TV-) model coefficients by exploiting an optimized Kalman-filter approach available online [16], which automatically estimates optimal model order with Akaike's Information criterion. We excluded the first 65 seconds of each acquisition to ensure a resting-state baseline during which subjects were relaxed. Then, we used a burn-in period of 100 samples (i.e., 25s) for the initialization of the Kalman filter. Thus, for each subject we analyzed a total of 5 minutes and 30 seconds made up of 90 seconds of open-eyes resting-state, 120 seconds of closed-eyes resting-state and 120 seconds of task. Then, we estimated Generalized Autoregressive Conditional Heteroskedasticity (GARCH) models on model error term to optimally track TV- residual

covariance matrix [16]. Indeed, temporal heteroskedasticity represents a major issue in the estimation of coupling measures obtained from TV-MVAR models, leading to inaccuracies in both strength and direction of coupling estimates. The obtained model coefficients along with residual covariance matrices were used to estimate the Directed Coherence (DC, [30]) in a TV- fashion. In particular, given the TV-MVAR model:

$$x_t = \sum_{k=1}^{p} A_k(t)x_{t-k} + \epsilon(t) \tag{1}$$

where $A_k(t)$ are the MxM coefficients matrices of the model at lag k and time t, and $\epsilon(t)$ is the error term at time t such that:

$$\epsilon_i(t) \sim \mathcal{N}(0, \sigma_i(t)). \tag{2}$$

Given:

$$\bar{A}(f) = I - \sum_{k=1}^{p} A_k(t)e^{-i2\pi fk} = I - A(f). \tag{3}$$

where $A(f)$ is the spectral representation of the coefficient matrix $A(t)$.

Being:

$$H(f) = [I - A(f)]^{-1} = \bar{A}(f)^{-1} \tag{4}$$

the transfer matrix associated with the MVAR model.

Then, the DC is given by:

$$DC_{ij}(f,t) = \frac{\sigma_j(t)H_{ij}(f,t)}{\sqrt{\sum_{m=1}^{M} \sigma_m^2(t)|H_{im}(f,t)|^2}} \tag{5}$$

Finally, since this measure is complex-valued, the modulus or the squared modulus are commonly used to measure connectivity in the frequency domain [29], [46].

DC was obtained in the $(0, f_{Nyquist})$ frequency range. Then, since the PNS contribution to HRV is between 0.15 and 0.40 Hz, and the SNS contribution to EDA is between 0.045 and 0.25 Hz, we only considered the DC values of their shared spectrum, i.e., the (0.15, 0.25) Hz frequency range. By doing so, we guarantee that only interpretable physiological interactions are observed.

D. Hypothesis testing of causal interactions

To evaluate the statistical significance of observed causalities, we developed an *ad-hoc* bootstrap procedure. Specifically, we extended the procedures presented in [32] and [33] to the case of TV-MVAR models with TV residuals. The procedure is based on resampling the model residuals thus allowing to get the empirical DC distribution under the null hypothesis of absence of causal interactions for a group of subjects and for a bivariate model. The following steps were performed:

a) For each subject, we fitted TV-MVAR models on HRV-EDA time series, and tracked TV model residuals using Generalized Autoregressive Conditional Heteroskedasticity (GARCH) modeling [16].

b) For each time-point, we estimated the DC in the $(0, f_{Nyquist})$ frequency range, and integrated in the desired frequency range (i.e., 0.15-0.25 Hz).

c) We calculated the median DC across subjects at each time-point (observed DC).

d) For each subject, we randomly resampled with replacement of the residuals obtained at step a.

e) We tested for the influence of time series j to i, by constructing a model where the MVAR coefficients $a_{ij}^{(k)}, k = 1, ..., p$ were set to zero, while the remaining coefficients were those originally estimated by TV-MVAR.

f) We generated a bootstrap multivariate time-series by using the resampled residuals of step d and the model coefficients of step e.

g) We built a surrogate time-series made of the modulus of the Fourier transform of the original time-series and the phase of the time-series generated at step f according to [33]. These time-series, which preserved the power spectra of the original time-series, corresponded to the surrogates under the null hypothesis of absence of causality from time series j to i.

h) For each bootstrap estimate, we calculated the median across subjects for each direction of interaction and time-point, obtaining a DC value for each (i, j, t) with $i \neq j$.

i) We repeated steps d - h until the desired number of bootstrap samples was reached.

j) Once the surrogate distribution was obtained, we associated to each observed DC a p-value, based on the position of the observed value in the bootstrap distribution.

In this work, we performed 3800 bootstrap estimates. Then, since we obtained a bootstrap distribution for each direction of interaction (i, j) with $i \neq j$, frequency (f) and time-point (t) we accounted for multiple testing hypotheses by correcting the observed p-values with the false discovery rate (FDR) procedure described in [47].

Finally, since the inversion of (4) could be computationally expensive, we estimated DC values as described in the Appendix.

III. RESULTS

In this section, for both protocols, we will present the observed Granger Causal interactions between EDA and HRV time series. In Fig. 3, we report the spectral representation of $|DC|$, while in Fig. 4 we integrate $|DC|$ in the (0.15-0.25) Hz frequency band, where EDA and HRV reflect the activity of the SNS and PNS, respectively. For the sake of clarity, we use $HRV \rightarrow EDA$ and $EDA \rightarrow HRV$ notation to indicate the direction of the observed causalities between the two signals (Fig. 4).

The results showed comparable behavior in the two resting conditions of the two experiments, which in both cases strongly differed with respect to the stressful session (i.e., HG or MC). This was also observed in terms of TV-model error (Fig. 5). Specifically, after the onset of the stressful task, the interaction between the two signals showed radical changes both in terms of directionality and dynamics. Moreover, the timing of these changes seems to strongly characterize the two types of stressful tasks. Indeed, faster dynamics of the $EDA \rightarrow HRV$ interaction as well as a faster baseline recovery were observed during the HG with respect to the

MC (Fig. 4). In the following sections, a detailed description of $HRV \rightarrow EDA$ and $EDA \rightarrow HRV$ dynamical causalities is reported.

A. Handgrip task

Significant causal interactions were investigated at the group level during the whole experiment. The median model order across subjects was $p = 2$ in the range of $(2 - 4)$. In Fig. 3 we report the time-frequency representation of $|DC|$ while in Fig. 4 we report the median averaged $|DC|$ time-courses for $HRV \rightarrow EDA$ and $EDA \rightarrow HRV$ that were statistically significant ($p < 0.05$, FDR corrected).

$HRV \rightarrow EDA$ causal interaction was significant during the rest conditions. On the other hand, no interactions were observed in the opposite direction (i.e., $EDA \rightarrow HRV$). After the onset of the HG task, the dynamics of HRV-EDA interactions changed from the rest. First, a peak in $HRV \rightarrow EDA$ was observed, at $\sim 8s$ from HG beginning. Then, such a causal interaction turned off after $\sim 5s$ from the observed peak and no significant interactions were observed for a small transient ($\sim 11s$), in none of the directions. After this transient, significant $EDA \rightarrow HRV$ occurred, whereas the influence of HRV over EDA was still suppressed. The $EDA \rightarrow HRV$ lasted $\sim 10s$ and then turned off. Finally, another $\sim 15s$-long transient with no interactions was present, until the $HRV \rightarrow EDA$ interaction was recovered.

B. Mental computation task

In Fig. 3 we report the spectral representation of median $|DC|$ across subjects. In Fig. 4 we also report the time-courses of $|DC|$ for $HRV \rightarrow EDA$ and $EDA \rightarrow HRV$ causal interactions that were significant ($p < 0.05$, FDR corrected). Also for MC, model orders were distributed in the range of $(2 - 4)$ with median of $p = 2$

During the rest condition, we observed a similar behavior as for the HG experimental protocol both in terms of full $|DC|$ spectra (Fig. 3) and HRV-EDA causal interactions (Fig. 4). Indeed, during rest the $|DC|$ spectral representation of $HRV \rightarrow EDA$ and $EDA \rightarrow HRV$ were comparable. Moreover, the influence of HRV over EDA was significant, while interactions in the opposite direction (i.e., $EDA \rightarrow HRV$) were not significant, confirming the replicability of results during the resting condition.

Likewise HG stressor, the dynamics of causal interactions changed after the onset of the MC stressful task in a similar fashion, but with different timing. Specifically, the $HRV \rightarrow EDA$ became not significant after $\sim 16s$ from the beginning of the MC, showing a remarkable peak after $\sim 8s$ as for the HG task. Afterwards, a $\sim 16s$ time-window without interactions occurred before the onset of an $EDA \rightarrow HRV$ interaction phase, which lasted for $\sim 24s$. Finally, in the last part of the MC session no significant causalities were observed except for two small peaks of $HRV \rightarrow EDA$.

IV. Discussion

In this study, we propose an *ad-hoc* methodological approach to investigate the dynamical causal interactions between the PNS and SNS based on EDA and HRV time-series. These are the most widely used signals for the non-invasive and unobtrusive characterization of the ANS dynamics and are able to selectively quantify the activity of SNS and PNS. The proposed approach integrates TV-MVAR modeling of EDA and HRV time-series, with the DC estimator, which enables to incorporate the *a priori* physiological knowledge by means of an appropriate choice of the frequency range contributing to the PNS-SNS interaction. To the best of our knowledge, this is the first causal modeling of sympathovagal interactions based on EDA and heart-beat dynamics.

Tracking changes in experimental conditions, as well as during the transition between conditions, should be the ultimate goal of causality analysis between coupled biological systems. TV solutions for MVAR model identification were consistently developed in the literature, aiming to obtain TV causal estimates between physiological time-series [48]. We exploited an optimized Kalman filter approach to fit MVAR models dynamically, allowing to track potential changes in the interaction between the two systems [16]. Furthermore, we controlled for heteroskedasticity of model residuals with the aim of reducing potential bias introduced by inaccurate error covariance matrices in DC estimates. Indeed, in real situations, changes in measurement noise, unobserved external factors or event-related changes and experimental phase transitions that are associated with different signal to noise ratio (SNR) levels, lead to inaccurate estimation of the strength and directionality of underlying couplings [16].

Another crucial point to be considered is that biological systems usually operate and interact each other through specific frequency bands. We incorporated the physiological knowledge about PNS and SNS dynamics taking advantage of the rigorous frequency representation of MVAR model coefficients given by the DC. Particularly, we analyzed the (0.15-0.25) Hz frequency range, that corresponds to the spectral overlap between the main sympathetic contribute to the EDA signal (i.e., EDASymp, 0.045-0.25 Hz) [12] and the only-parasympathetic part of the HRV signal (i.e., HF, 0.15-0.4 Hz) [4]. Specifically, instead of operating with spectral quantities of HRV and EDA [40], we directly model the whole range of possible interactions between the EDA and HRV time-series, and then we integrate such interactions in the frequency range of interest. In fact, if spectral causalities are required, values outside the frequency range of interest may simply be ignored, while appropriate time-domain causalities may be obtained by averaging spectral causalities over the frequency range of prior interest [49].

Furthermore, we took into account another physiological knowledge concerning the temporal dynamics of the EDA generation process. Specifically, we shifted the EDA by -1.62s to take into account for the physiological delay between the onset of SNS discharge and the sweat secretion that generates the EDA signal. Indeed, since the overall concept of Granger Causality is based on the assumption that cause precedes effects [19], a constant delay between the measured signals could heavily impact on the direction of causal profiles. Simulation studies addressed this issue by temporally shifting time-series based on previously estimated latencies. Hence, GC estimates were improved in terms of true

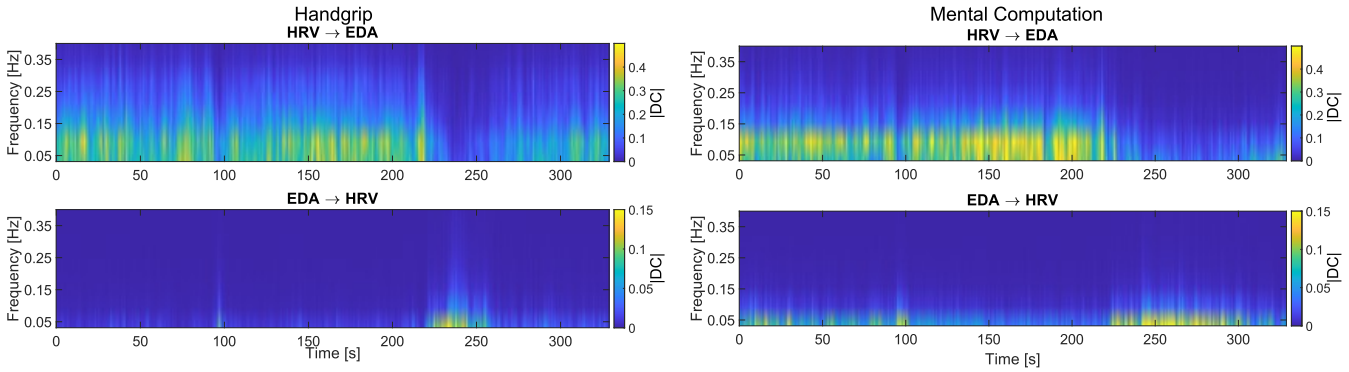

Fig. 3. **Spectral representation of $|DC|$.** (left) Group-level median $|DC|$ during the Handgrip task. (right) Group-level median $|DC|$ during the Mental Computation task.

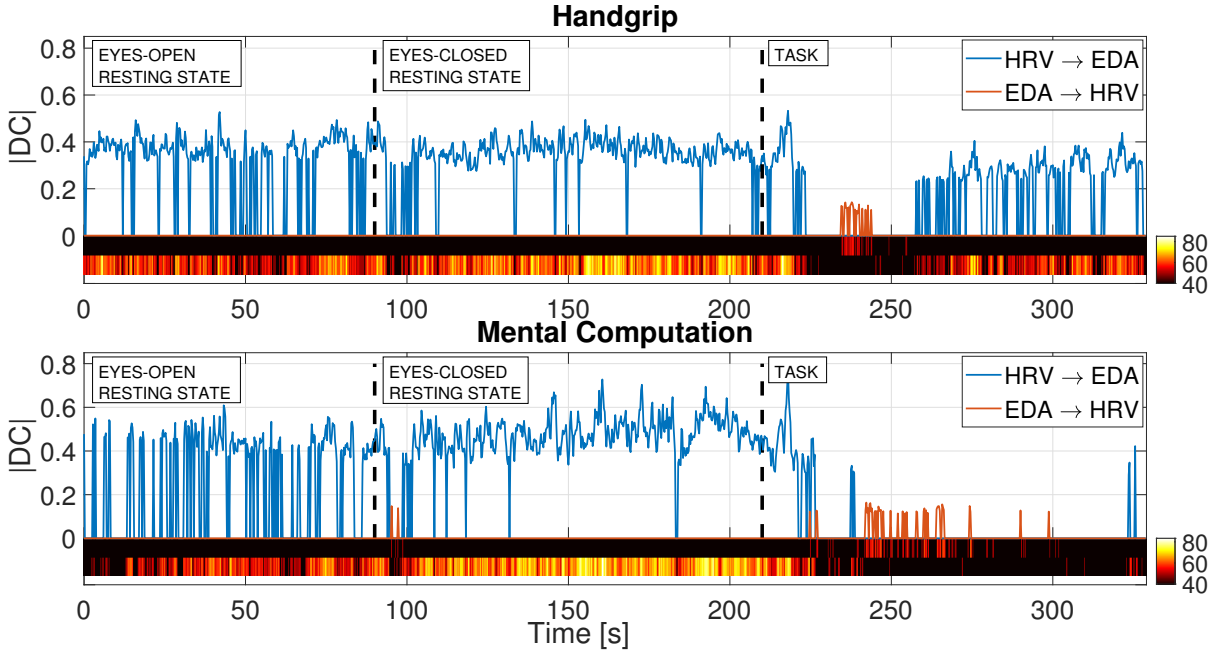

Fig. 4. **Causal interactions during Handgrip and Mental Computations tasks.** (top) Group-level median-average significant ($p < 0.05$, FDR corrected) $|DC|$ values integrated in the (0.15-0.25) Hz frequency range during the Handgrip task. (bottom) Group-level median-average significant ($p < 0.05$, FDR corrected) $|DC|$ values integrated in the (0.15-0.25) Hz frequency range during the Mental Computation. Vertical lines correspond to eyes closing and to the start of the task. At the bottom of each plot we report, for each time-point, the % of subjects for which the interaction was significant at the subject level. The top row corresponds to $EDA \rightarrow HRV$ causality, while the bottom row corresponds to $HRV \rightarrow EDA$ causality.

detected interactions [45]. Here, on the one hand, considering that our sampling time was 250ms, we assumed that the differences in conduction time of the vagal and sudomotor nerves (controlling the heart and sweat gland activity) were comparable [50], [51]. On the other hand, the delay between the sweat gland nerve stimulation and the sweat secretion process (i.e., the EDA signal generation) is not negligible [44]. Based on the delay reported in [44], we shifted the EDA by -1.62s, i.e., the average delay associated with tactile stimulation. The latter not only was the most similar stimulus to those adopted in our study (partially sharing the autonomic neural paths involved in the HG task) but also the one with the lowest delay among those reported in [44]. Accordingly, it can be considered a conservative choice. Indeed, in this way, we limited the potential risk of introducing instantaneous interactions in the model due to overestimated time-shifts.

Another potential issue of shifting time-series for causal analysis is to ensure that small changes of the delay, as for instance the subject-specific variability, do not affect the causal estimates. In our case, the subject-specific differences were estimated to be within our sampling interval (i.e., $T_s = 250ms$) [44]. Therefore, we assumed that the stability of results is guaranteed under these limits. Yet, for different delays and different sampling intervals, such assumptions may not hold, requiring proper validation.

Additionally, we provided along with our method, an *ad-*

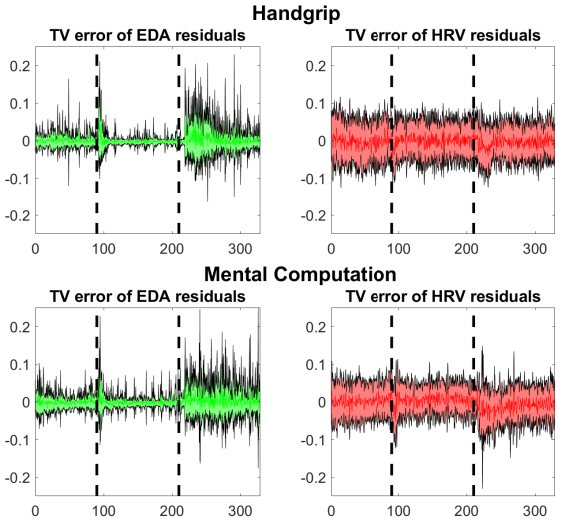

Fig. 5. **Mean ± std of the estimated TV model error of EDA and HRV time-series.** (top) Group-level median-average TV-model error during the Handgrip task. (bottom) Group-level median-average TV-model error during the Mental Computation task. Vertical lines correspond to eyes closing and to the start of the task. TV-model errors follow transitions from rest to task.

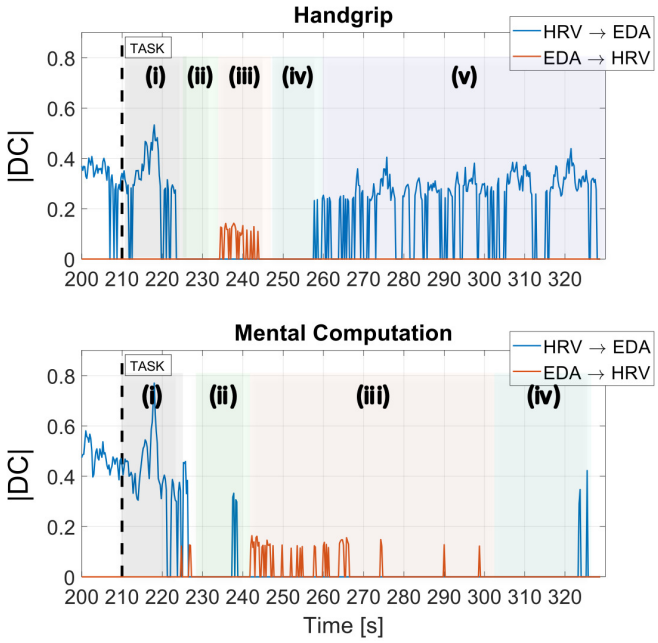

Fig. 6. **Different phases of causal interactions following Handgrip and Mental Computations tasks.** (i) peak in $PNS \rightarrow SNS$ causal interaction, (ii) absence of interactions, (iii) $SNS \rightarrow PNS$ causal interaction, (iv) absence of interactions, (v) only for HG, baseline recovery (v). (top) Different phases of interactions highlighted above group-level median-average DC values in the (0.15-0.25) frequency range during the Handgrip task. (bottom) Different phases of interactions highlighted above group-level median-average DC values in the (0.15-0.25) frequency range during the Mental Computation task.

hoc statistical framework for the estimation of true causalities at the group level in the case of TV model coefficients and TV residual variances. Specifically, group-level TV DC was obtained by median averaging subject-specific DC values for each direction of interaction, frequency and time-point. In this context, algorithmic procedures to obtain the distribution of causal measures have been developed [33]. Here, we extended such algorithmic solutions to the case of TV MVAR models with heteroskedastic residuals. Specifically, being an extension of the bootstrap procedures available in [32], [33], [41], the proposed approach can be applied independently on the distribution of the data.

Among the several types of normalization of MVAR model coefficients, we focused here on the Directed Coherence [30]. Accordingly, we obtained frequency-domain causal estimates that could be interpreted in terms of transmitted power spectrum from one process to another [29], [30], [46].

Our method was applied to two standard protocols, i.e., HG and MC, which are known to trigger a sympathetic response by increasing the arousal level. However, although they are both considered sympathetic activation tasks, the underlying regulatory mechanisms can be different as well as the interaction dynamics between the two ANS branches [52], [53].

The proposed approach allowed us to obtain physiologically plausible interactions and showed good replicability of the results. Indeed, it is worthwhile noting that our results both in terms of EDA and HRV power spectrum (Fig. 2), $|DC|$ spectral properties (Fig. 3), and PNS-SNS causal influence (Fig. 4) were replicable across the two experiments when the resting condition was considered. Specifically, for both experiments, only $HRV \rightarrow EDA$ causality was significant at rest. Since the PNS constantly regulates bodily functions mainly through vagal activity in resting conditions [54], we can hypothesize that observing only $HRV \rightarrow EDA$ causality at rest may reflect the suppression of the SNS activity performed by the vagal tone. Moreover, the interactions that occurred after the beginning of each stressful task followed the similar cascade of events: (i) a peak in $PNS \rightarrow SNS$ causal interaction, (ii) absence of interactions, (iii) $SNS \rightarrow PNS$ causal interaction, (iv) absence of interactions (Fig. 6). For the HG we could also observe a phase of baseline recovery (v) at the end of the task (i.e., $PNS \rightarrow SNS$).

This specific sequence of events could reflect the dynamics related to the control of stressful stimuli by the ANS. In fact, previous physiological studies on HG response have proved that static HG elicits a cardiovascular pressor response that does not immediately correspond to a sympathetic activation being initially sustained by a vagal withdrawal [52]. This seems to be controlled at the central nervous system level during the early stages of the task (i.e., up to 30s), while for longer durations, sensory and metabolic signals from the muscles strongly activate the sympathetic component thus increasing the sympathetic outflow [52]. Interestingly, although (i) and (ii) phases were very similar between the HG and MC tasks, the (iii) and (iv) phases took place with different timing. Indeed, on the one hand, both HG and MC responses similarly show a peak after $\sim 8s$ in the $PNS \rightarrow SNS$ interaction as well a subsequent time window without significant

coupling. On the other hand, the HG response differed from the MC one because it induced a lower duration of both the $SNS \rightarrow PNS$ phase ($\sim 10s$ vs $\sim 24s$, i.e., phase (iii)) and of the following time window without significant interactions (i.e., phase iv). Such differences may reflect the activation of different autonomic regulatory routes. At speculation level, mental stress might show slower dynamics due to the complex top-down regulatory processing which arises at central level in the central autonomic network [55], which orchestrates central stress inputs from the brainstem and other subcortical and cortical structures including, among others, the insula, amygdala, and hypothalamus. Moreover, the baseline recovery, clearly observable during the HG task, was not evident in the case of the MC (where a $PNS \rightarrow SNS$ significant interaction started only at the very end of the MC task). It is likely that participants have not been able to sustain the maximal effort for the whole task period. In fact, as reported in the final interview, they experienced muscle fatigue in the second part of the HG task that could have reduced the effort and the associated SNS firing, thus limiting the $SNS \rightarrow PNS$ phase to a very short period corresponding to the real time interval in which maximal force was applied and strong SNS activation occurred. This is in line with previous studies that showed that maximal and submaximal (80%) isometric contraction can be effectively sustained for short time periods (e.g., maximal force for 16s) [52]. In contrast, it is likely that the cognitive activity required for MC could be sustained for the whole task as suggested by previous findings showing that during longlasting arithmetical tasks SNS firing went on throughout the whole session [53].

It is worthwhile noting that we did not observe simultaneous causalities in both directions (i.e., $PNS \rightarrow SNS$ and $SNS \rightarrow PNS$), although non-reciprocal interactions between the two systems have been suggested [4]. In this view, due to the impossibility to compare our results with a ground-truth measure (e.g., microneurography), our approach might be unable to model some interactions, as for instance nonlinear coupling, which often reflects physiological mechanisms [4], [15]. Indeed, although linear models were found to be satisfactory in describing some kind of nonlinear couplings [20], we should also consider that those cases may not cover the entire range of potential complex interactions of PNS and SNS. Accordingly, future improvements will integrate nonlinear estimates MVAR model coefficients [15], [56] along with TV solutions, in order to track linear and nonlinear couplings in a TV fashion. A further limitation could be also due to the integration of the observed causalities in the (0.15-0.25) Hz frequency range. In fact, this might offer only a partial view of the true underlying interactions: on the one hand, the PNS contribution to the lower frequencies of the HRV is excluded [4]; on the other hand, the SNS contribution represented by the low frequencies of the EDA signal is partially discarded [9]. Particularly, most of the EDA power is below 0.15 Hz (Fig. 2), therefore it is likely to assume that such components could explain other PNS-SNS interactions, which cannot be captured by our modeling approach. Yet, our assumptions are crucial for the interpretability of the results. Indeed, at low frequencies, it would not possible to distinguish the nature of the ongoing interaction (i.e., $PNS_{HRV} - SNS_{EDA}$ vs. $SNS_{HRV} - SNS_{EDA}$), as the LF of HRV, is influenced by both PNS and SNS. Accordingly, future developments should investigate PNS-SNS interactions also at lower frequencies.

Another relevant consideration should involve the role of respiratory activity in the modulation of the investigated causal interactions. The HF power spectrum of HRV may be influenced by the respiration activity such that changes in the respiration pattern could have an impact on causal estimates. However, previous studies have proven that the modulation of respiration over heart rate diminishes during exercise [57], when respiratory frequency increases. Here, we hypothesized that the same applied to HG and MC. In fact, the mean respiratory frequency throughout the tasks resulted outside the considered frequency threshold of 0.25 Hz. Accordingly, we assumed that the effects of respiration on the causality analysis could be neglected. Yet, we also believe that future developments could include respiratory signals in the model.

Of note, the evaluation and interpretation of our results is also helped by the experimental paradigms used in this work, which were chosen to convey predictable responses of the PNS and SNS. The physiological plausibility of the observed causalities suggest that our modeling approach successfully identified the driving effect of one system over the other at rest and during stressful tasks. However, we believe that future work should include more complex situations known to trigger autonomic response, as for instance those provided by emotional stimuli and/or social interactions. In particular, since the characterization of PNS-SNS interactions in such situations may be nontrivial, well-established methods for estimating causality will be needed.

V. Conclusion

This work offers for the first time a method for estimating PNS-SNS causal interactions starting from EDA and HRV signals. We integrated the *a priori* physiological knowledge of PNS and SNS contributions to HRV and EDA with sophisticated causal modeling of time-series to infer causal interactions between the two branches of the autonomic nervous system in response to two different stressful tasks. The replicability of our physiologically-sound results is encouraging for studying of PNS-SNS interactions in more complex scenarios. Particularly, it is our view that the proposed method would pave new roads in the study of PNS-SNS interactions in response to emotional tasks, as well as to the investigation of interaction alterations typical of cardiovascular, inflammatory, metabolic, neurological, and psychiatric disorders.

VI. Appendix

In the following lines, we report a brief practical proof of the equivalence between $|DC_{ij}(f)|$ and $|gPDC_{ij}(f)|$ for $i \neq j$ and $M = 2$.

Given a set of simultaneously observed time-series

$$X(n) = [x_1(n) \dots x_M(n)]^T \tag{6}$$

Given the MVAR model of order p that adequately represents $X(n)$:

$$\begin{bmatrix} x_1(n) \\ \vdots \\ x_M(n) \end{bmatrix} = \sum_{r=1}^{p} A_r \begin{bmatrix} x_1(n-r) \\ \vdots \\ x_M(n-r) \end{bmatrix} + \begin{bmatrix} \epsilon_1(n) \\ \vdots \\ \epsilon_M(n) \end{bmatrix} \tag{7}$$

with

$$A_r = \begin{bmatrix} a_{11}(r) & a_{12}(r) & \dots & \dots & a_{1M}(r) \\ \vdots & \vdots & \vdots & \vdots & \vdots \\ \vdots & \vdots & \vdots & a_{ij}(r) & \vdots \\ \vdots & \vdots & \vdots & \vdots & \vdots \\ a_{M1} & \dots & \dots & \dots & a_{MM}(r) \end{bmatrix} \tag{8}$$

where the coefficients $a_{ij}(r)$ represent the linear interaction effect of $x_j(n-r)$ onto $x_i(n)$.

Given the Fourier transform of MVAR model coefficients of (8):

$$A(f) = \sum_{r=1}^{p} A_r e^{-i2\pi fr} \tag{9}$$

Then, the gPDC estimator is given by [58]:

$$gPDC_{ij}(f) = \frac{\frac{1}{\sigma_i}\bar{A}_{ij}(f)}{\sqrt{\sum_{k=1}^{M} \frac{1}{\sigma_k^2}\bar{A}_{kj}(f)\bar{A}_{kj}^*(f)}} \tag{10}$$

where

$$\bar{A}_{ij}(f) = I - A_{ij}(f). \tag{11}$$

We recall the definition of the DC [30]:

$$DC_{ij}(f) = \frac{\sigma_j H_{ij}(f)}{\sqrt{\sum_{k=1}^{M} \sigma_k^2 |H_{ik}(f)|^2}} \tag{12}$$

where

$$H^{-1}(f) = \bar{A}(f) \tag{13}$$

Then, we explicit eq. (10) for the bivariate case (i.e., $M = 2$):

$$|gPDC_{12}(f)| = \frac{\frac{1}{\sigma_1}|\bar{A}_{12}(f)|}{\sqrt{\frac{1}{\sigma_1^2}|\bar{A}_{12}|^2(f) + \frac{1}{\sigma_2^2}|\bar{A}_{22}(f)|^2}} \tag{14}$$

and we substitute $\bar{A}(f)$ with $H^{-1}(f)$ according to:

$$\begin{aligned} H^{-1}(f) &= \frac{1}{\det H} \begin{bmatrix} H_{22}(f) & -H_{12}(f) \\ -H_{21}(f) & H_{11}(f) \end{bmatrix} \\ &= \begin{bmatrix} \bar{A}_{11}(f) & \bar{A}_{12}(f) \\ \bar{A}_{21}(f) & \bar{A}_{22}(f) \end{bmatrix} = \bar{A}(f) \end{aligned} \tag{15}$$

which leads to:

$$|gPDC_{12}(f)| = |DC_{12}(f)| \tag{16}$$

The same procedure can be used to find

$$|gPDC_{21}(f)| = |DC_{21}(f)| \tag{17}$$

Of note: the equivalence does not hold for the elements on the diagonal of $\bar{A}_{ij}(f)$, since $\bar{A}_{11}(f)$ is proportional to H_{22} and $\bar{A}_{22}(f)$ is proportional to H_{11}.

Given (16) and (17), it is possible to estimate DC by using (10) and avoiding the inversion of (13). In particular, this is computational advantageous in the case of small data samples and/or time-varying scenarios [58].

REFERENCES

[1] L. K. McCorry, "Physiology of the autonomic nervous system," *American journal of pharmaceutical education*, vol. 71, no. 4, p. 78, 2007.

[2] M. N. Levy, "Brief reviews: sympathetic-parasympathetic interactions in the heart," *Circulation research*, vol. 29, no. 5, pp. 437–445, 1971.

[3] K. Ondicova and B. Mravec, "Multilevel interactions between the sympathetic and parasympathetic nervous systems: a minireview," *Endocr Regul*, vol. 44, no. 2, pp. 69–75, 2010.

[4] F. Shaffer and J. P. Ginsberg, "An Overview of Heart Rate Variability Metrics and Norms," *Frontiers in Public Health*, vol. 5, p. 258, Sep. 2017.

[5] Electrophysiology Task Force of the European Society of Cardiology the North American Society of Pacing, "Heart Rate Variability," *Circulation*, vol. 93, no. 5, pp. 1043–1065, Mar. 1996, publisher: American Heart Association.

[6] Society for Psychophysiological Research Ad Hoc Committee on Electrodermal Measures, "Publication recommendations for electrodermal measurements: Publication standards for EDA," *Psychophysiology*, vol. 49, no. 8, pp. 1017–1034, Aug. 2012.

[7] R. Freeman and M. W. Chapleau, "Testing the autonomic nervous system," in *Handbook of Clinical Neurology*. Elsevier, 2013, vol. 115, pp. 115–136.

[8] H. F. Posada-Quintero, et al., "Analysis of Reproducibility of Noninvasive Measures of Sympathetic Autonomic Control Based on Electrodermal Activity and Heart Rate Variability," *IEEE Access*, vol. 7, pp. 22 523–22 531, 2019.

[9] H. F. Posada-Quintero, et al., "Time-varying analysis of electrodermal activity during exercise," *PLOS ONE*, vol. 13, no. 6, p. e0198328, Jun. 2018.

[10] A. Greco, G. Valenza, and E. P. Scilingo, *Advances in Electrodermal activity processing with applications for mental health*. Springer, 2016.

[11] W. Boucsein, *Electrodermal activity*. Springer Science & Business Media, 2012.

[12] H. F. Posada-Quintero, et al., "Power spectral density analysis of electrodermal activity for sympathetic function assessment," *Annals of biomedical engineering*, vol. 44, no. 10, pp. 3124–3135, 2016.

[13] H. F. Posada-Quintero, et al., "Time-varying analysis of electrodermal activity during exercise," *PloS one*, vol. 13, no. 6, p. e0198328, 2018.

[14] S. Ghiasi, et al., "Assessing Autonomic Function from Electrodermal Activity and Heart Rate Variability During Cold-Pressor Test and Emotional Challenge," *Scientific Reports*, vol. 10, no. 1, p. 5406, Dec. 2020.

[15] L. Faes, G. Nollo, and K. H. Chon, "Assessment of Granger Causality by Nonlinear Model Identification: Application to Short-term Cardiovascular Variability," *Annals of Biomedical Engineering*, vol. 36, no. 3, pp. 381–395, Mar. 2008.

[16] K. Kostoglou, et al., "A novel framework for estimating time-varying multivariate autoregressive models and application to cardiovascular responses to acute exercise," *IEEE Transactions on Biomedical Engineering*, 2019.

[17] H. Lütkepohl, *New Introduction to Multiple Time Series Analysis*. Springer Science & Business Media, Dec. 2005.

[18] N. Wiener, "The theory of prediction," *Modern Mathematics for Engineers*, 956.

[19] C. W. J. Granger, "Investigating causal relations by econometric models and cross-spectral methods," *Econometrica*, vol. 37, no. 3, pp. 424–438, 1969.

[20] B. Schelter, et al., "Testing for directed influences among neural signals using partial directed coherence," *Journal of Neuroscience Methods*, vol. 152, no. 1, pp. 210 – 219, 2006.

[21] S. L. Bressler and A. K. Seth, "Wiener–granger causality: A well established methodology," *NeuroImage*, vol. 58, no. 2, pp. 323 – 329, 2011.

[22] C. Granger and P. Newbold, "Spurious regressions in econometrics," *Journal of Econometrics*, vol. 2, no. 2, pp. 111 – 120, 1974.

[23] M. Ding, et al., "Short-window spectral analysis of cortical event-related potentials by adaptive multivariate autoregressive modeling: data preprocessing, model validation, and variability assessment," *Biological Cybernetics*, vol. 83, no. 1, pp. 35–45, Jun. 2000.

[24] W. Hesse, et al., "The use of time-variant eeg granger causality for inspecting directed interdependencies of neural assemblies," *Journal of Neuroscience Methods*, vol. 124, no. 1, pp. 27 – 44, 2003.

[25] T. Milde, et al., "A new kalman filter approach for the estimation of high-dimensional time-variant multivariate ar models and its application in analysis of laser-evoked brain potentials," *NeuroImage*, vol. 50, no. 3, pp. 960 – 969, 2010.

[26] K. J. Blinowska, "Review of the methods of determination of directed connectivity from multichannel data," *Medical & Biological Engineering & Computing*, vol. 49, no. 5, pp. 521–529, May 2011.

[27] R. D. Pascual-Marqui, et al., "Assessing direct paths of intracortical causal information flow of oscillatory activity with the isolated effective coherence (icoh)," *Frontiers in human neuroscience*, vol. 8, p. 448, 2014.

[28] S. Cekic, D. Grandjean, and O. Renaud, "Time, frequency, and time-varying Granger-causality measures in neuroscience," *Statistics in Medicine*, vol. 37, no. 11, pp. 1910–1931, May 2018.

[29] L. Faes, S. Erla, and G. Nollo, "Measuring connectivity in linear multivariate processes: definitions, interpretation, and practical analysis," *Computational and mathematical methods in medicine*, vol. 2012, 2012.

[30] L. Baccala, et al., "Studying the interaction between brain structures via directed coherence and granger causality," *Applied signal processing*, vol. 5, no. 1, p. 40, 1998.

[31] L. A. Baccalá, D. Y. Takahashi, and K. Sameshima, *Computer Intensive Testing for the Influence Between Time Series*. John Wiley & Sons, Ltd, 2006, ch. 16, pp. 411–436.

[32] J. R. Sato, et al., "Frequency domain connectivity identification: An application of partial directed coherence in fMRI," *Human Brain Mapping*, vol. 30, no. 2, pp. 452–461, Feb. 2009.

[33] L. Faes, A. Porta, and G. Nollo, "Testing frequency-domain causality in multivariate time series," *IEEE Transactions on Biomedical Engineering*, vol. 57, no. 8, pp. 1897–1906, 2010.

[34] A. Porta, et al., "Multimodal signal processing for the analysis of cardiovascular variability," *Philosophical Transactions of the Royal Society A: Mathematical, Physical and Engineering Sciences*, vol. 367, no. 1887, pp. 391–409, Jan. 2009, publisher: Royal Society.

[35] L. Faes, G. Nollo, and K. H. Chon, "Linear and nonlinear parametric model identification to assess granger causality in short-term cardiovascular interactions," in *2008 Computers in Cardiology*, 2008, pp. 793–796.

[36] L. Faes, G. Nollo, and A. Porta, "Mechanisms of causal interaction between short-term rr interval and systolic arterial pressure oscillations during orthostatic challenge," *Journal of Applied Physiology*, vol. 114, no. 12, pp. 1657–1667, 2013.

[37] C. Corbier, et al., "Causal analyses to study autonomic regulation during acute head-out water immersion, head-down tilt and supine position," *Experimental Physiology*, vol. 105, no. 8, pp. 1216–1222, 2020.

[38] A. Porta, et al., A. Cividjan, and L. Quintin, "Cardiovascular control and time domain Granger causality: insights from selective autonomic blockade," *Philosophical Transactions of the Royal Society A: Mathematical, Physical and Engineering Sciences*, vol. 371, no. 1997, p. 20120161, Aug. 2013, publisher: Royal Society.

[39] A. Porta, et al., "Disentangling cardiovascular control mechanisms during head-down tilt via joint transfer entropy and self-entropy decompositions," *Frontiers in Physiology*, vol. 6, Oct. 2015.

[40] A. L. Callara, et al., "A preliminary study on parasympathetic-sympathetic interaction through the analysis of heart rate variability and electrodermal activity," in *2020 11th Conference of the European Study Group on Cardiovascular Oscillations (ESGCO)*, 2020, pp. 1–2.

[41] M. Havlicek, et al., "Dynamic granger causality based on kalman filter for evaluation of functional network connectivity in fmri data," *NeuroImage*, vol. 53, no. 1, pp. 65 – 77, 2010.

[42] H. Sedghamiz, "Matlab implementation of pan tompkins ecg qrs detector," *Code Available at the File Exchange Site of MathWorks*, 2014.

[43] A. Greco, et al., "cvxeda: A convex optimization approach to electrodermal activity processing," *IEEE Transactions on Biomedical Engineering*, vol. 63, no. 4, pp. 797–804, 2015.

[44] R. Sjouwerman and T. B. Lonsdorf, "Latency of skin conductance responses across stimulus modalities," *Psychophysiology*, vol. 56, no. 4, p. e13307, Apr. 2019.

[45] C. Chang, M. E. Thomason, and G. H. Glover, "Mapping and correction of vascular hemodynamic latency in the bold signal," *NeuroImage*, vol. 43, no. 1, pp. 90 – 102, 2008.

[46] L. A. Baccalá and K. Sameshima, "Partial directed coherence: a new concept in neural structure determination," *Biological cybernetics*, vol. 84, no. 6, pp. 463–474, 2001.

[47] J. D. Storey and R. Tibshirani, "Statistical significance for genomewide studies," *Proceedings of the National Academy of Sciences*, vol. 100, no. 16, pp. 9440–9445, Aug. 2003.

[48] M. F. Pagnotta and G. Plomp, "Time-varying mvar algorithms for directed connectivity analysis: Critical comparison in simulations and benchmark eeg data," *PLOS ONE*, vol. 13, no. 6, pp. 1–27, 06 2018.

[49] L. Barnett and A. K. Seth, "The mvgc multivariate granger causality toolbox: A new approach to granger-causal inference," *Journal of Neuroscience Methods*, vol. 223, pp. 50 – 68, 2014.

[50] L. Parisi, et al., "Estimation of the conduction velocity of sympathetic sudomotor c fibers in healthy subjects: study of sympathetic skin reflex," *Funct. Neurol.*, vol. 16, pp. 231–237, 2001.

[51] K. Y. Qing, et al., "B fibers are the best predictors of cardiac activity during Vagus nerve stimulation: Qing, vagal B fiber activation and cardiac effects," *Bioelectronic Medicine*, vol. 4, no. 1, p. 5, Dec. 2018.

[52] P. M. Macey, et al., "Sex differences in insular cortex gyri responses to a brief static handgrip challenge," *Biology of Sex Differences*, vol. 8, no. 1, p. 13, Dec. 2017.

[53] M. D. Muller, C. L. Sauder, and C. A. Ray, "Mental stress elicits sustained and reproducible increases in skin sympathetic nerve activity," *Physiological Reports*, vol. 1, no. 1, Jun. 2013.

[54] J. F. Thayer and R. D. Lane, "Claude bernard and the heart–brain connection: Further elaboration of a model of neurovisceral integration," *Neuroscience & Biobehavioral Reviews*, vol. 33, no. 2, pp. 81–88, 2009.

[55] F. Beissner, et al., "The autonomic brain: an activation likelihood estimation meta-analysis for central processing of autonomic function," *Journal of neuroscience*, vol. 33, no. 25, pp. 10 503–10 511, 2013.

[56] D. Marinazzo, et al., "Nonlinear connectivity by granger causality," *NeuroImage*, vol. 58, no. 2, pp. 330 – 338, 2011.

[57] D. A. Kenwright, et al., "The effect of low-frequency oscillations on cardio-respiratory synchronization," *The European Physical Journal B*, vol. 65, no. 3, pp. 425–433, 2008.

[58] L. A. Baccala, K. Sameshima, and D. Y. Takahashi, "Generalized Partial Directed Coherence," in *2007 15th International Conference on Digital Signal Processing*, Jul. 2007, pp. 163–166, iSSN: 1546-1874, 2165-3577.